

FAILURE ANALYSIS AND HOT TEARING SUSCEPTIBILITY OF STAINLESS STEEL CF3M

Dheeraj S. Bhiogade, Sanjay M. Randiwe, and Abhaykumar M. Kuthe

Department of Mechanical Engineering, CAD/CAM, Visvesvaraya National Institute of Technology, Nagpur, India

Copyright © 2018 American Foundry Society
<https://doi.org/10.1007/s40962-018-0246-z>

Abstract

Hot tear formation has been witnessed during the solidification of the ferrous alloy by pulling the columnar dendrites in the transverse direction. The hot tearing susceptibility of an alloy is influenced by solidification rate, microstructure and the stress/strain conditions. It is valuable to predict the occurrence of tearing in a casting. In this study, hot tearing susceptibility of stainless steel CF3M grade casting was investigated using the method of constrained T-shaped solidification shrinkage and inducing strain by pulling dendrites in a transverse direction. An experimental setup equipped with the real-time measurement of temperature, displacement and contraction/applied force during solidification at elevated temperature has been developed. In this study, the sectioning technique was adopted for residual stress measurement after casting solidification, wire electric discharge machining has been identified as a suitable method of cutting along with a coordinate measuring machine sufficiently accurate for

measurement, and finite element modeling and analysis were performed to calculate the stress. A metallographic study using an optical microscope and scanning electron microscope was performed to evaluate macro- and microstructure at failure zone of the casting. The study aims to investigate crack morphology and differentiate hot tear from other types of cracks in order to troubleshoot effectively. Stress, strain and temperature data provide onset of hot tearing and provide a base for mathematical model and validation. The results show that the strain or strain rate is more critical for hot tearing than stress. The studies on residual stress show that the tensile stress is not required to generate hot tears, but only the tensile strain is sufficient to form a hot tear.

Keywords: hot tear, stainless steel CF3M (316L), residual stress, metallographic study, crack morphology

Introduction

Hot tearing is one of the most detrimental casting solidification defects.¹ Hot tearing, in the form of cracks, occurs at or above the solidus temperature during solidification of metal casting. The shapes and appearance of hot tear defects depend on both the local state of stress and interdendritic feeding. Concerning mechanical properties, the material in the mushy state can be regarded as a porous metallic material saturated with its liquid phase.² Three critical temperatures are closely related to the strength of the alloy during alloy solidification, i.e., coherence temperature, coalescence temperature and rigidity temperature.^{3,4} Due to the thermal contraction of the solid phase during alloy solidification, stress can build up after the dendritic network is coherent, dendrites begin to interact each other, and the granular solids form in the semi-solid zones. In addition, stresses build up in casting

regions due to the geometric constraint of the mold. The interdendritic liquid flow takes place to compensate for solidification shrinkage, thermal contraction and local deformation of the solid phase. When the interdendritic liquid flow can feed these local deformation regions, in which dendrite arms are pulled apart over a significant distance, the space between displaced dendrite arms is filled, and the hot tears are healed. As solidification proceeds, the solid fraction increases, the area open for interdendritic fluid flow decreases, and liquid feeding of solidification shrinkage becomes more difficult. Thus, at high-volume fraction of solid, an opening of the dendritic network caused by tensile deformation is likely to remain unfilled, allowing cracks to nucleate and grow, and causing a hot tear defect.⁵ Causes for hot tears initiation in castings are the stresses developed during cooling, isolated hot spots, uneven thermal gradients in casting, constriction stress caused by mold or core, low melt-point

phases in the interdendritic regions, high pouring temperatures and metal chemistry. Owing to the complex mechanisms acting during the solidification of metals, prediction of a hot tearing phenomenon is not an easy task. Mechanical behavior of CF3M above solidus temperature had not been studied. This study focused on experimental setup and technology concerned with high-temperature testing which facilitated the characterization of material properties, i.e., strength of material in terms of stress and strain at temperature encountered during casting process. These test results led to the formulation of the complex computational model for hot tearing.

Over the years some of the studies on hot tearing attempted to reveal its characteristics. Most notably, Pellini,⁶ was concerned with strain theory and concept of liquid films. Thomas,⁷ revealed that hot tearing occurs near the solidus temperatures due to the combination of tensile stress and metallurgical embrittlement. Campbell¹ postulated that a hot tear was a uniaxial tensile failure in weak portion of material and suggested theories related to bifilm for initiation of defect. Clyne and Davies⁸ revealed that the strain can be accommodated during liquid and mass feeding and will occur during the last stage of solidification. Shimin Li et al. reviewed paper theories of hot tearing; hot tearing variables; and test methods to predict hot tearing of aluminum alloy.⁹ A summary of hot tearing criteria/models is also provided. It was concluded that hot tearing is a complex phenomenon that involves heat flow, melt flow and mass flow, as well as the development of stresses/strains in the coherent network. Also it was stated that none of the existing models can predict whether hot tearing will occur or not. A robust and reliable hot tearing prediction model is still not available. Reliable quantitative measurement of hot tearing, as well as reliable modeling and prediction of hot tearing, will be of great value to the casting industry. Hot tear modeling becomes more demanding due to its complexity of mushy zone.¹⁰ Several hot tearing criteria have been implemented in simulation of metal casting with the commercial software, such as ProCAST,^{11–13} MAGMASoft,¹⁴ and ABAQUS.¹⁵ The finite difference method (FDM) is more efficient for flow analyses, while finite element method (FEM) is more accurate below the solidus temperature. Some of the researchers simulated the high-strength alloys Co–Cr hip resurfacing prosthesis with ProCAST.¹³ Simulated location of hot tears and shrinkage porosity and the severity of hot tearing are in agreement with the casting practice. Pokorny et al.¹⁴ validated a viscoplastic model to simulate the hot tear with MAGMASoft in AZ91D permanent mold casting. The predicted damage from the simulations was found to be in good agreement with the hot tears observed in the experiments in terms of both location and severity. A recent criterion that was developed for solidification cracking during welding was also applied for estimating hot tearing during casting.^{16, 17} Lin et al. developed a new mechanical model to

predict the hot tearing of steel castings in green sand molds. In the analysis, they used the methods developed by Metzger et al. and Chan and Dantzig to take into account the restraint force in green sand molds.¹⁸

In addition to the theoretical analysis and formulations, casting engineers have developed cast house tests to evaluate hot tearing tendency by acquiring load, temperature and displacement data during casting solidification. Many other researchers have carried out extensive work in this arena^{19–22} on a variety of systems and also in an attempt to quantify hot tearing tendency. Zhi-Qiang Wei et al.²³ demonstrated the hot tearing susceptibility of the duplex stainless steel (DSS). They developed setup equipped with thermocouple and stress sensor, acquired data from sample melted and held at 1560 °C for 5 min and then allowed to solidify in the crucible made up of Al₂O₃. Graphs of stress and temperature with respect to time were recorded and it was concluded that when the temperature in the core of sample arrives at the liquidus temperature, its contraction stress is dramatically increased because the temperature of most of the molten steel is already below the coalescence temperature, and the resistance against contraction strain is enhanced effectively. It was also stated that when the core is at 50% solid fraction, the contraction stress is released; at that time, hot tearing susceptibility is largest and least for 2 s with temperature reduction of 2 °C. Zhijun Li et al.²⁴ investigated the effect of cooling rate on hot-crack behavior and influences on ferrite/austenite ratio of DSS. This study revealed that when the cooling rate decreases from 6 to 1 °C/s, the coarse dendritic microstructure of austenite in DSS is changed gradually into isolated-island shapes and the ferrite/austenite ratio decreases from 2.3 to 1.25 as well, while the linear contraction rate increases from 1.59 to 1.9%. The decrease in ferrite/austenite ratio in DSS, i.e., increase in austenite content, encourages its hot-crack susceptibility. A. Stangeland,²⁵ demonstrated that hot tearing susceptibility depends on liquid pressure drop and development of viscoplastic strain for Al–Cu binary alloy by experimentation and simulation. And it was concluded that changing the parameters in the constitutive equation for thermal strain will result in changes in the viscoplastic strain and liquid pressure drop that have opposite effects on the hot tearing susceptibility. The net effect on the hot tearing susceptibility is small. H. Akhyar et al.²⁶ evaluated hot tearing susceptibility (HTS) using qualitative experiments of constrained rod casting modified-horizontal molds in a combination of three casting temperatures and four aluminum alloys. The HTS equation was developed to evaluate the hot tearing tendency of metal by the length of bars, tear categories and tear position. In recent research, the hot tearing susceptibility of stainless steel CF3M has been studied, and results have revealed that with an increasing degree of superheat, the hot tearing susceptibility increased. And it was suggested that viscoplastic constitutive model was

Table 1. Elemental Composition of the CF3M Casted Samples

Elements	Carbon (C)	Chromium (Cr)	Copper (Cu)	Iron (Fe)	Manganese (Mn)	Nickel (Ni)	Molybdenum (Mo)	Sulfur (S)	Phosphorus (P)
Test sample (wt%)	0.03	16.66	0.39	68.83	1.55	10.13	2.023	0.0147	0.0289

used to predict the hot tear and an accumulated plastic strain.²⁷ Few researchers had investigated hot tearing on Al–Cu multi-component alloys and revealed that the alloys with nominal high Cu content of 7.3 and 8 wt% Cu were the most hot tear resistant.²⁸ Tuttle et al. pointed out the reduced segregation and hot tearing when aluminum alloys are grain refined. Despite these observed improvements, grain refinement has not been applied to steel alloys. It reveals that the TiN and TiC particles would have a good crystallographic match to δ -ferrite which supports the idea that it acted as nuclei for some of the primary dendrites. Purposely introducing or forming many TiN particles will reduce the grain size of castings leading to improved mechanical properties.²⁹

Most studies have focused only on nonferrous alloy castings such as aluminum and aluminum alloy, until recently limited work on ferrous casting like stainless steel has been carried out. Type SS316L is commonly used in the human body as prosthesis because of its bio-acceptability as an implant.³⁰ ASTM (American Society for Testing and Materials)-type CF3M is the cast equivalent of 316L (S31603). And cast implants should exhibit certain properties such as yield strength, fatigue strength, ductility, hardness and toughness, surface tension and surface energy, tensile, compressive and shear strength as per requisite ASTM standards. This study was focused on hot tear analysis of high-strength ferrous casting and high-temperature testing machine for real-time data acquisition which is further supportive for the development of a computational model of the hot tear. In this study, the constraint T-shaped casting of a ferrous alloy similar to CF3M was investigated for hot tearing susceptibility. Experimentation was performed using casting prepared in SiO₂ sand mold cored by CO₂, poured at 1560 °C, tested on five different test conditions and strain inducing on casting were recorded forces, temperatures, and displacements with respect to time and data was processed for hot tear analysis and prediction. As per our previous research, the numerical model was validated using simulation.²⁷ The torn casted samples were tested for metallurgical analysis and also tested for residual stress analysis assisted by wire cut electro-discharge machining (WEDM) and heat treatments. The study provided the data regarding the alloy's physical and chemical changes that occurred due to the application of ultimate or breaking force during solidification and also provided insight into hot tearing in CF3M alloy.

Experimental Method

Experimental Material

Elemental composition of the alloy similar to CF3M was obtained by spectrometer test (type CF3M is the cast equivalent of SS316L) of a material sample tested as per ASTM E 1086:2008 methods listed in Table 1.

Experimentation

The constrained T-shaped casting experimental setup used in this study was developed at Visvesvaraya National Institute of Technology (VNIT), Nagpur, Maharashtra (India). The experimental setup bears a close resemblance to one proposed by Monroe and Beckermann.¹⁵ The experimental setup was also stated in our previous research.²⁷ An approach to investigate hot tearing is to measure the exerted force and induced strain during solidification of steel alloy at high temperature. The test setup used for tests is depicted in Figure 1a, b. T-shape selected for experimental casting and simulation has 300-mm-long arms and a 100-mm-long and 25-mm-thick leg as depicted in Figure 2a. Stainless steel bolt is anchored into a cavity in order to measure contraction force and induce strain, shown in Figure 2b. The devices were set up in order to acquire temperature, force and displacement data. Setup was equipped with measurement devices, i.e., K-type and B-type thermocouples, S-type load cell, the loading device and data acquisition system (DAQ). Temperatures in mold were measured using 100-mm spade K-type temperature controller thermocouple sensor, 5-mm-diameter probe, and 1-m-long cable, and temperature at casting was measured using Type B thermocouple with joint composition as platinum 30% rhodium and platinum 6% rhodium. Two thermocouples are being placed in hot spot zone: T1 (Type B) and T2 (Type K) as shown in Figure 1a. Force data were acquired with a 15KN S-type load cell, having sensitivity: 2.0 ± 0.05 mV/V, shown in Figure 3a mounted on right side of the casting. Experimental data were collected using a data acquisition system shown in Figure 3b.

The molds were made using silica sand (SiO₂) bonded with a sodium silicate binder (Grade NTL-30) and CO₂ gas as a catalyst agent. The molten steel was prepared in a 15-KW (Electrotherm) induction furnace having 5 kg capacity and poured at a temperature about 1560 °C with the help of

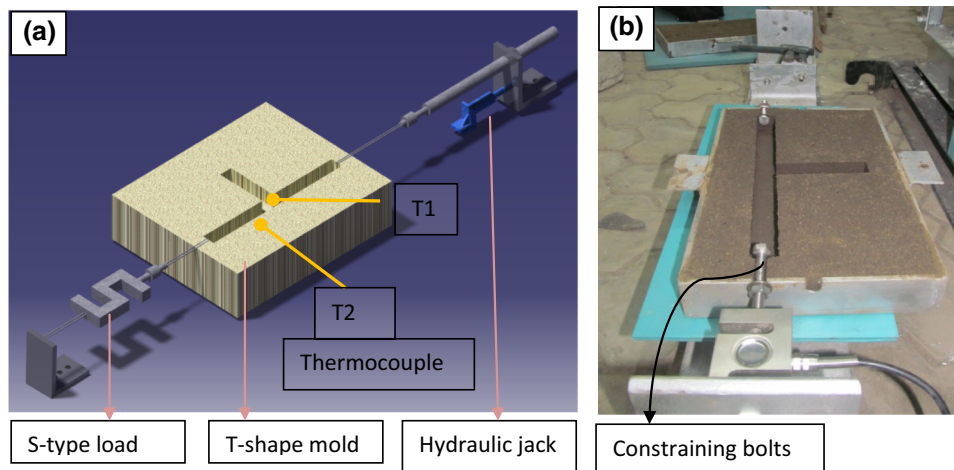


Figure 1. (a) Schematic of the experimental setup of T-shaped casting, (b) experimental instrumented setup.

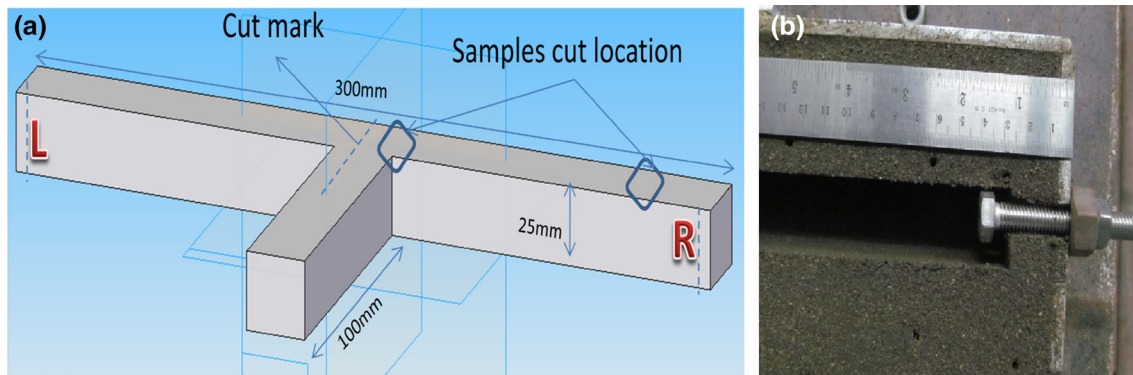


Figure 2. (a) T-shaped pattern 3D model for experiment and simulation, (b) constrain bolt anchoring into the cavity.

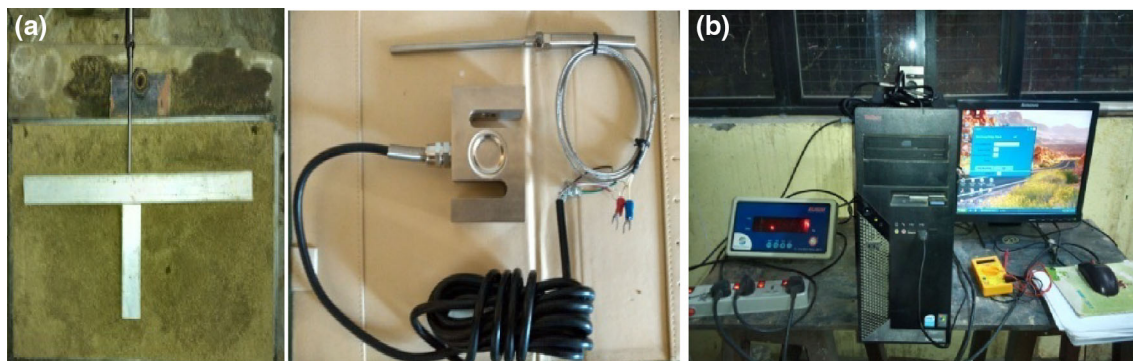


Figure 3. (a) Mold along with S-type load cell and thermocouple, (b) data acquisition system (DAQ) setup.

auto-pour machine in order to maintain the constant flow rate of molten steel into the mold cavity. When the molten metal was poured into the T-shaped cavity of the silica sand mold, rapid solidification around the steel bolts can transfer the tensile forces between the casting and the S-type load cell. And then, the unidirectional tensile forces

are applied; as we know, hot tearing initiation and propagation were directly related to the presence of the force or stress and strain, so control over the magnitude of the applied force was necessary. The magnitude and rate of applied force are controlled by the horizontal hydraulic jack. A jack is connected to the left side of casting opposite

Table 2. Casting Experiments Measured and Simulation Parameters and Test Conditions

Test conditions	Test 1	Test 2	Test 3	Test 4	Test 5	
Pouring temperature 1560 °C, Pouring rate (0.7–1.25 kg/s), Total filling time (Avg. 1.80 S), Solidification time (3 min)	Free contraction	Auto-cast Simulation	Free contraction with displacement measurement	Constrained by load bolt and tightening	Constrained by hydraulic jack and load cell	Constrained by load cell and pull by hydraulic jack

to load cell. Tensile forces are applied at a predetermined rate until the specimen fractures. During experimentation, five different test conditions were considered for data collection and failure analysis, as shown in Table 2, and in tests 1 and 2, castings were free to contract without any constraint, i.e., unrestrained casting experiments; this was for initial benchmark readings required for comparing with casting simulation results; during test 1, only temperature readings were recorded with respect to time using two thermocouples (T1 and T2). In test 2, casting was free to contract and displacement was measurements with the help of LVDT (linear variable differential transformer) at each end of mold. A 3-mm-diameter quartz rod was connected at one end to LVDT, and the other end was inserted 3–5 mm into mold cavity. To avoid quartz rod slippage in the casting, end of the rod was bulged into a spherical shape using an oxy-acetylene torch. Quartz is a suitable material to use in this application because of its high melting point and low thermal expansion. Total length change in the bar was calculated by adding the displacements of two LVDTs. Tests 3, 4 and 5 were performed in order to constrain for contraction, i.e., strained casting experiments and initiate a hot tear in casting with the application of control magnitude of applied force. In test 3, casting experiments were performed by constraint with load bolts from both ends and force with respect to time was recorded. In test 4, they were performed with the application of static external force by hydraulic jack. In test 5, they were performed with dynamic application of external forces by hydraulic jack horizontal displacement, and readings were recorded for each experiment. At last, the castings or samples are taken out from the mold after full solidification and then examined. Each test was repeated 3 times. The data of temperatures and applied forces were simultaneously acquired by a recorder. After acquiring the data, the temperature curve and applied forces versus time curve are processed to obtain critical information for hot tearing formation.

In order to characterize the casting failure, the following methods were used: visual inspection, microscopic examination, and scanning electronic microscope (SEM). The samples were taken from T-junction, i.e., hot spot (failure zone) and from an end of the arm, sample cut locations are marked in Figure 2a. Samples were sectioned from the T shape of the castings for each condition. These samples were then ground using varying levels of SiC papers (i.e.,

120, 320 and 600 grit) and subsequently polished using 5- μm alumina, 3- μm diamond suspension and finally 1- μm diamond suspension. The measurements were taken on a metallurgical microscope in conjunction with image analysis software and camera. There are two samples (i.e., one from T-junction and one at the arm end) for each test condition. Further, analysis of secondary phases will be carried out using SEM.

The experimental measurements of the residual stress state can be taken adopting several methods, such as destructive and semi-destructive methods which are also called a mechanical method and nondestructive methods. Thorborg et al.³¹ adopted hole drilling technique to evaluate the residual stress state, but in their work they pointed out that such a methodology has a limited accuracy, since it was based on the transformation of information from the strain gauge response due to stress redistribution when the material is removed by drilling/removing material in the surface. Another method, i.e., sectioning technique, included in the group of the destructive techniques,^{32,33} was used for the experimental evaluation of the residual stress state: such a technique relies on the measurements of deformation due to the release of residual stress upon the removal of material from the specimen. In order to minimize material alterations due to the cutting, the electro-discharge machining (EDM) process was used, and the stress release after the cutting was measured in terms of displacements with respect to a physical reference mark. And contour method, also a part of sectioning technique, was numerically verified by 2D finite element (FE) simulation and experimentally validated on a bent steel beam having a known residual stress distribution.³⁴ The result obtained from the contour method was in excellent quantitative agreement with the outcome measured by neutron diffraction technique.

In this study, the sectioning technique was adopted for residual stress measurement. Application of the sectioning technique involves four steps: specimen cutting, measurement, data reduction and stress analysis. Specimen cutting was the first and most critical step, and the subsequent procedures of measurement, data reduction and stress analysis are all reliant on the quality of the cutting. Wire electric discharge machining has been identified as a suitable method of cutting of specimen,³³ as it uses electrical discharges (sparks) instead of hard cutting tools to remove

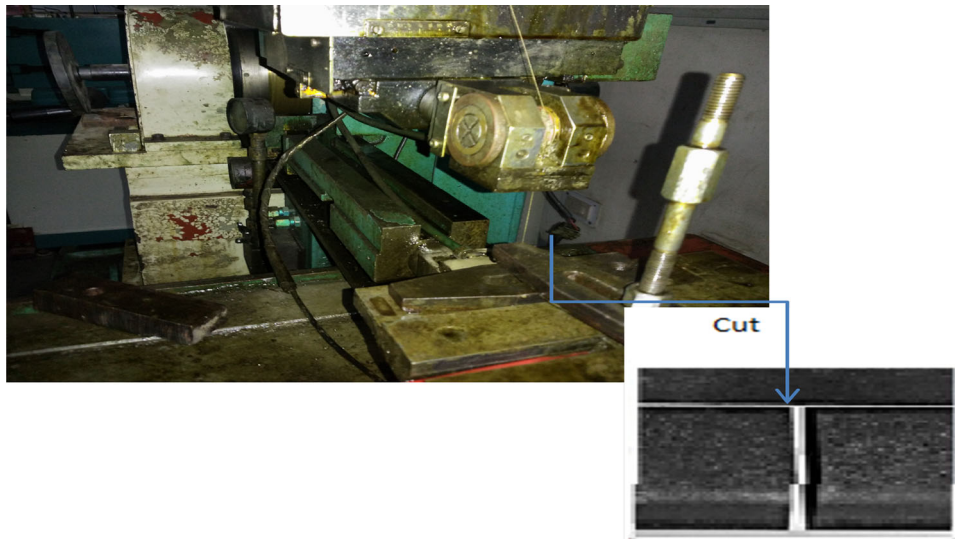


Figure 4. Wire electric discharge machining along with casting cut, and wire position before and after cut.

material. The cut was positioned at the center of the T-junction as shown in Figure 2a, and the reference marks L and R are also shown. Following the specimen cutting, the stress release after the cutting was measured in terms of displacements with respect to a physical reference mark and wire as shown in Figure 4. A coordinate measuring machine (CMM) has been proved to be sufficiently accurate for measurement.³⁴ A CMM was designed to measure complex shapes with high precision. The deflection of the stylus triggers a computer to record the position of each contact point. After acquiring data the data smoothed by data reduction technique and subsequently finite element modeling and analysis were performed to calculate the original stress.

Results and Discussion

Initial investigation of CF3M grade casting for susceptibility to hot tearing due to pouring temperature was

conducted in previous research.²⁷ Figure 5 shows the measured displacement vs. time curves for CF3M tested at a three different pouring temperatures, i.e., 1460, 1510 and 1560 °C. Figure 6 shows the stress with respect to time graphically; it was observed that the solidification of casting occurred with pouring temperatures 1460, 1510 and 1560 °C and the load started to develop at second, fourth and sixth seconds, respectively, and increased with time. From the data and the curves, for 1460, 1510 and 1560 °C solidification was complete at around 94, 111 and 128 s, respectively, the total linear shrinkage/contraction (displacement) of the solidification range is around 4.69, 4.89, and 5.08 mm compared to the length of the bar of 300 mm. This displacement is expected to correlate with the hot tearing susceptibility of the alloy. The result has revealed that with the increasing degree of superheat, the hot tearing susceptibility increased. The thermal and displacement history was used for casting simulation and thermo-physical properties calculations. As the force and displacement were density and Young's modulus driven parameters.

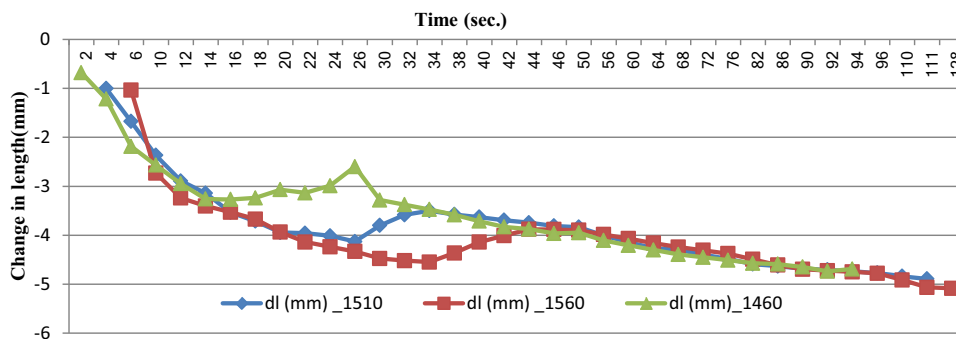


Figure 5. Measured displacement as a function of time.

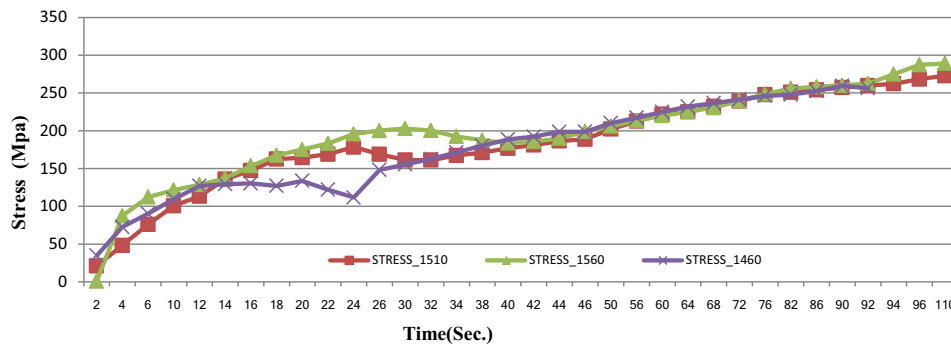


Figure 6. Stress induced during solidification with respect to time.

Viscoplastic constitutive model was used to predict the hot tear; and we have found that hot tearing is, in fact, the accumulated plastic strain.

In continuation with the effect of pouring temperature experimentation, the constraint T-shaped casting experiments were performed and pouring temperature was selected about 1560 °C. Load and displacement data measured from experiments are recorded and are represented graphically. Table 2 shows the five different test conditions and simulation parameters. In test 1 casting is free to contract without any constrain. This is for initial benchmark reading required for comparing with simulation result. In test 2 casting is free to contract with displacement measurement. Test 3, 4 and 5 is performed in order to constraint for contraction and form a hot tear in casting with the application of control magnitude of applied force, was achieved by hydraulic jack horizontal displacement.

Temperature data for test 1 and stresses for test 4 are collected. The fraction of solid, temperature and cooling

rate with respect to time are shown in Figure 7. Cooling rate and a fraction of solid are derived from casting simulation. It is found that the potential solidification heat is released and cooling slows down when the liquid is converted into solid. Molten steel is at a temperature of approximately 100 °C overhear, i.e., 1560 °C when the test begins. Temperature, stress and the first derivative of stress with respect to time curves are shown Figure 8. The recorded stress was transferred by two bolts placed at both ends in molten steel of T-shaped casting, giving a chilling effect which solidifies the ends first and when temperature further decreased, a solidification shell is formed on the surfaces of casting, which indicate some part of melt on the surface is cooled to the coalescence temperature or at rigidity temperature. Therefore, rods transmit force effectively to load cell. With the increase in solid fraction, the ability to resist deformation increases; therefore, stress increases rapidly with the increase in shrinkage. It can be seen that the stress release begins at the temperature of 1535 °C and ends at 1527 °C; at same time area which is solidified first has temperatures 1100 and 1058 °C,

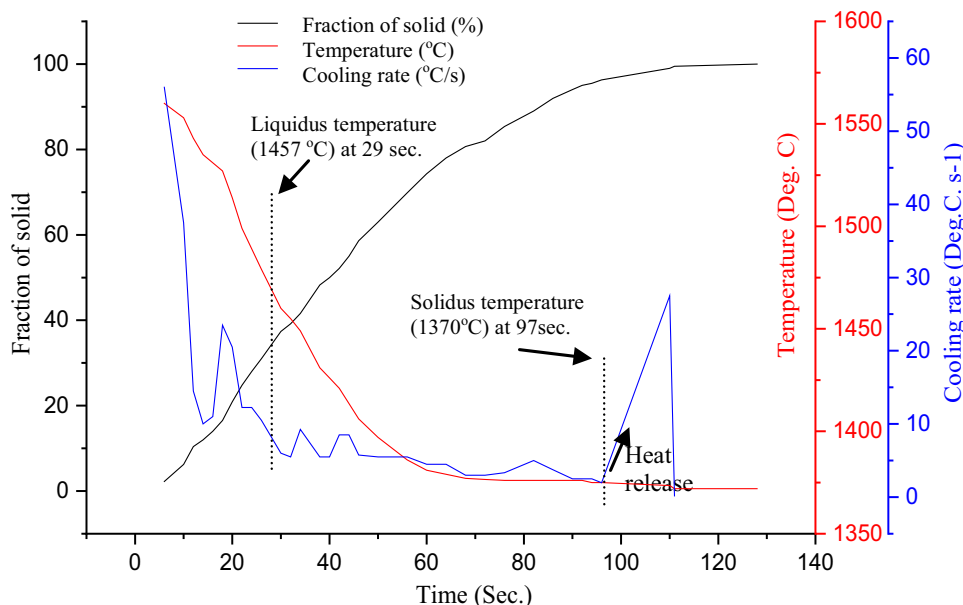


Figure 7. Fraction of solid, cooling curve and cooling rate.

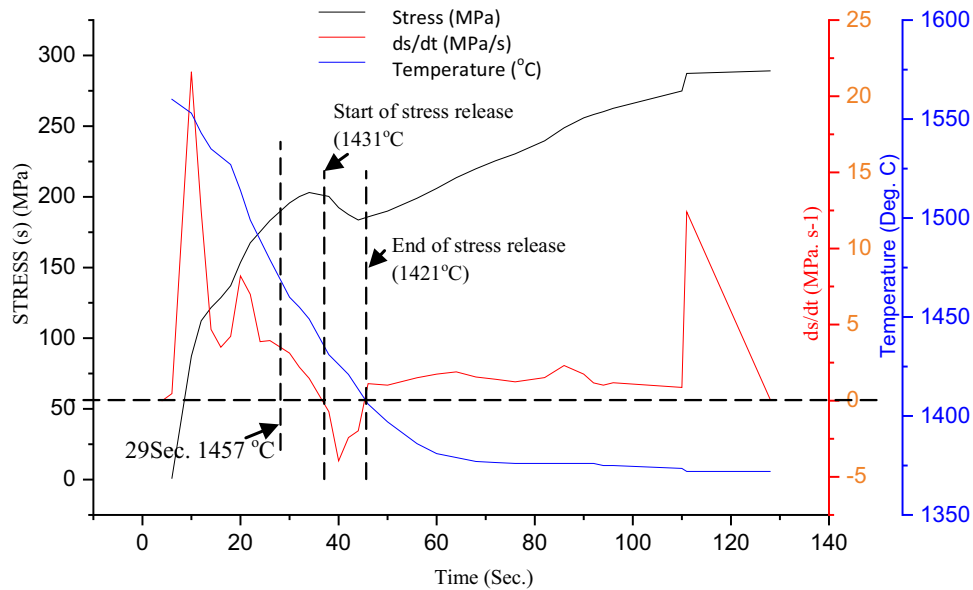


Figure 8. Temperature, stress and first derivative of stress with respect to time curves.

respectively. The temperature difference and the time duration in the stress release process are 7 °C and 4 s, respectively, which confirms the process of the tear formation and healing as shown in Figure 7; the simulation software shows that the solid fraction is about 16% in the range of 1535 to 1527 °C when the temperature of the molten steel decreases to the temperature of stress release. The same fluctuation of stress release observed in the same sample is shown in a graph in the temperature range of 1431 to 1421 °C; at that time the solid fraction is around 50% and time duration of 4 s is observed. When the solid fraction in the core approaches 50%, molten steel in the core is at mushy state. At this time, the hot tearing

susceptibility of the sample is largest. The sample was torn at second stress release point, and the first fluctuation represents the healed hot tear. Recorded stresses during solidification with respect to temperature are represented graphically in Figure 9 for last three test conditions, i.e., test 3, 4 and 5 as shown in Table 2. Each test was performed thrice, and two sets of readings are depicted in the graph. From stress to temperature graph, the onset of hot tear was calculated. Figure 10a, b depicts test 5 castings having hot tear, Figure 10c shows test 4 casting having crack observed after magnification, and Figure 10d shows test 3 casting with no significant defect observed.

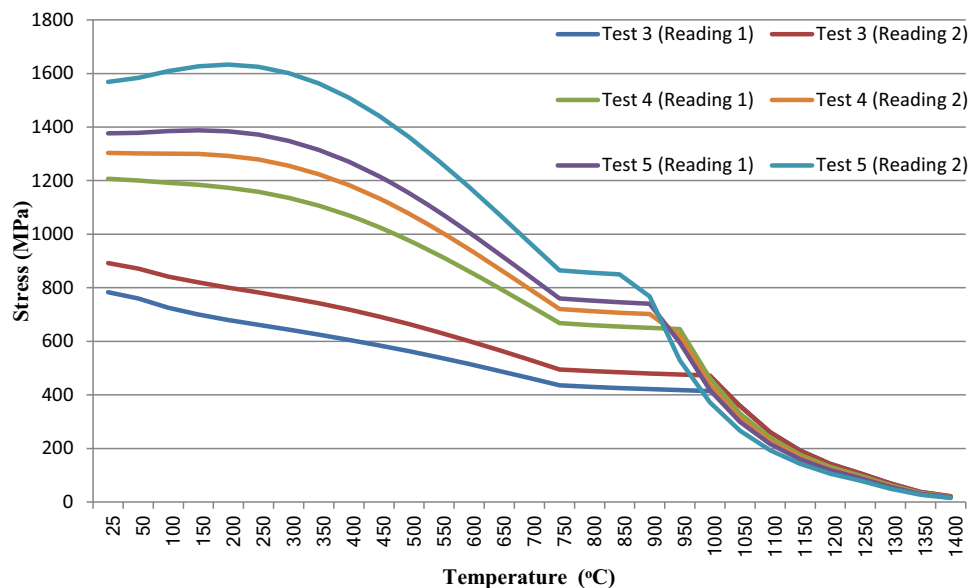


Figure 9. Recorded stresses with respect to temperature for different conditions.

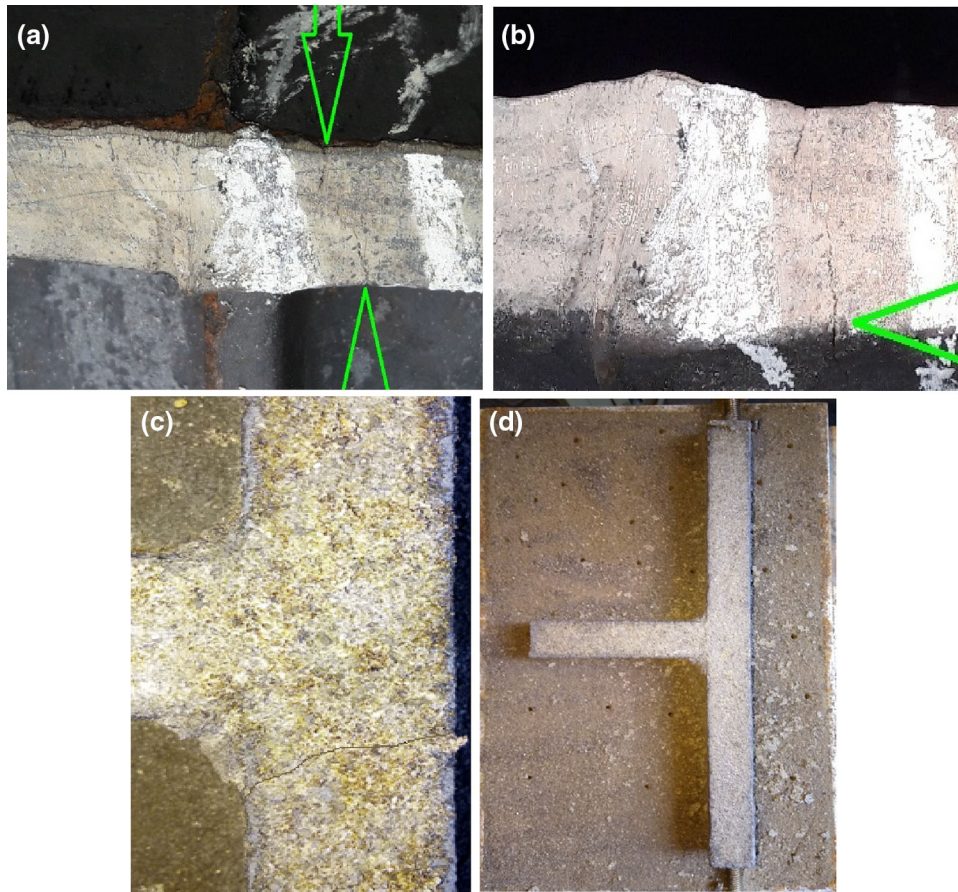


Figure 10. (a) and (b) Test 5 castings having hot tear c) Test 4 casting having crack observed after magnification d) Test 3 casting no significant defect observed.

In order to investigate residual stress in constrained casting after tear, the sectioning technique was adopted for residual stress measurement. Wire electric discharge machining has been used for cutting of T-shaped castings specimen. In the case of test 4 casting, a displacement of $0.0850 \pm 1E-4$ mm was measured; in the case of test 5 casting, the displacement of the side arms was much less, i.e., $0.0100 \pm 1E-4$ mm, and finite element modeling and analysis were performed to calculate the original stress.

Mathematical Models

The viscoplastic constitutive relations are estimated using data to derive the plastic strain and yield strain in the failure zone. Hot tear indicator (HT) is, in fact, the accumulated plastic strain ($\dot{\varepsilon}^{VP}$) expressed as Eqn. 1.

$$HT = \int \sqrt{2/3} \dot{\varepsilon}^{VP} : \dot{\varepsilon}^{VP} d\tau \quad \text{Eqn. 1}$$

Arrhenius equation has been used to express flow stress, especially at high temperatures; the strain rate can be express as Eqn. 2:

$$\dot{\varepsilon}_o = AF(\sigma) \exp\left(-\frac{Q}{RT}\right) \quad \text{Eqn. 2}$$

where $\dot{\varepsilon}_o$ is the reference strain rate, A is the Arrhenius pre-factor, Q is the activation energy, and R is the universal gas constant.

The most important mechanical characteristic of a material is its high strain rate sensitivity (m) of flow stress and can be expressed as Eqn. 3. The value of m was determined with the help of stress relaxation test, m is determined as the slope of the experimental stress versus strain rate plot, and the equation is derived for all temperature (T) as Eqn. 4.

$$\varepsilon_{eq} = \sigma_o + K(\dot{\varepsilon}_{eq})^m \quad \text{Eqn. 3}$$

$$\frac{1}{m} = 8.132 - 1.54 \times 10^{-3}T \quad \text{Eqn. 4}$$

The yield stress of the solid material is given by

$$\sigma_{dy} = \sigma_o \left(1 + \frac{\varepsilon_{eq}}{\varepsilon_o}\right)^n \left(1 - \frac{\dot{\varepsilon}_{eq}}{\dot{\varepsilon}_o}\right)^m \quad \text{Eqn. 5}$$

where σ_o is the initial yield stress, ε_{eq} is the equivalent plastic strain, ε_o is the reference shear strain and given by $\varepsilon_o = \frac{\sigma_o n}{E}$, $\dot{\varepsilon}_{eq}$ is the equivalent plastic strain rate, n is the strain hardening exponent, m is the strain rate sensitivity, and E is Young's modulus.

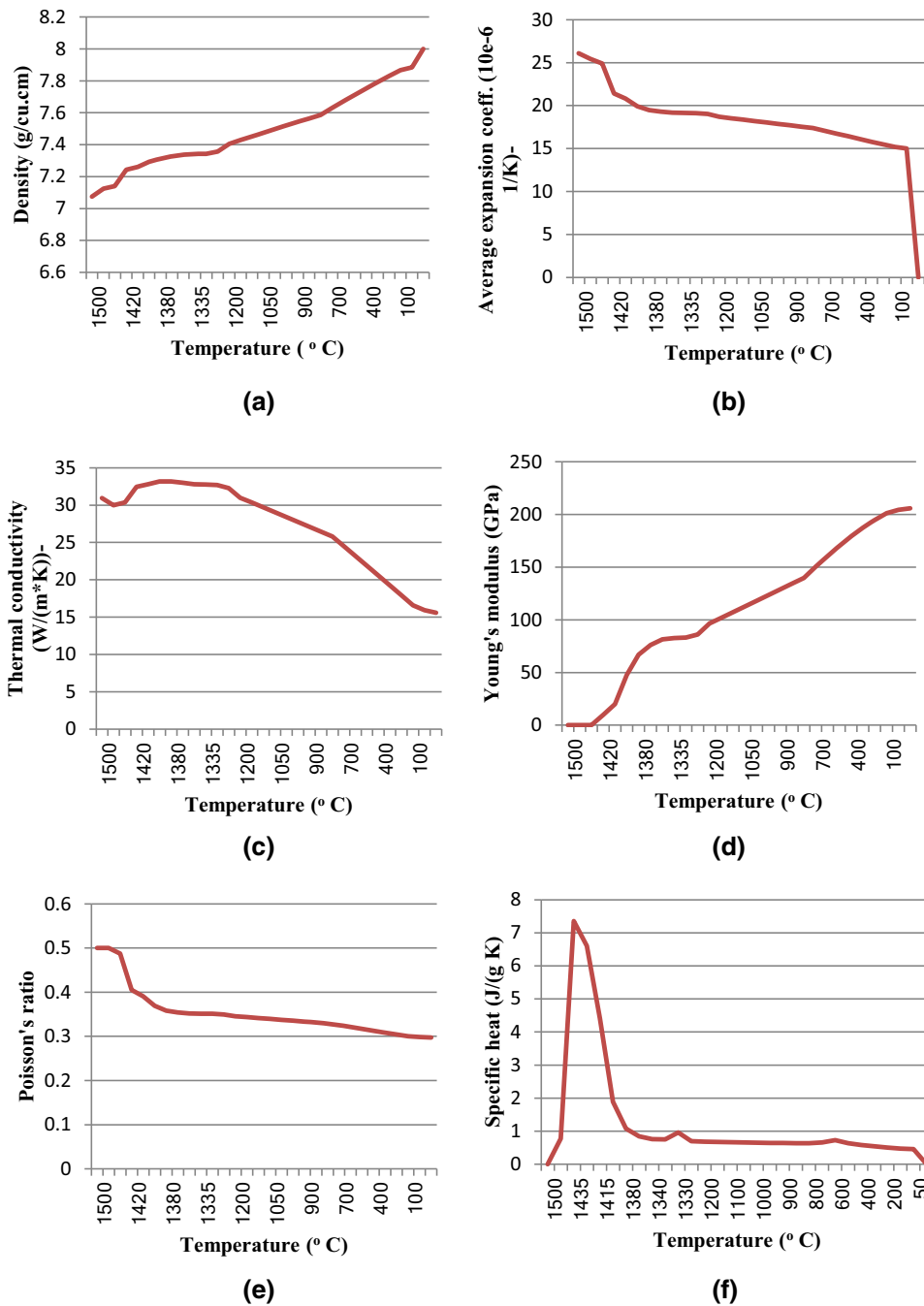


Figure 11. The temperature-dependent thermo-physical properties of CF3M. (a) Density (g/cm³), (b) average expansion coeff. (10e⁻⁶ 1/K), (c) thermal conductivity (W/(m * K), (d) Young's modulus (GPa) (e) Poisson's ratio (f) specific heat (J/(g K).

$$\dot{\epsilon}_{eq} = f_{\%c} (\sigma_{eq} - \sigma_o)^{\frac{1}{m}} \exp \left[-\frac{4.465 \times 10^4}{T} \right] \quad \text{Eqn. 6}$$

The unknown viscoplastic parameters of Eqns. 5 and 6 are σ_o , n , m , ϵ_o and $\dot{\epsilon}_o$. Three parameters (σ_o , n and m) were assumed to be linear functions of temperature. A is carbon content dependent and was assumed to be a quadratic function, and Q is a temperature independent constant and the value is 371.220 kJ/mol.

Strain hardening exponent (n) is the measure of increase in hardness and strength caused by plastic deformation; it approximated the relation between stress and strain during plastic deformation of a metal. Strain hardening occurred on a plastic zone of the stress–strain curve and it's followed the power law (i.e., $\sigma = K \epsilon^n$). Equation 7 is derived from the experimental stress–strain curve, and this equation helps to get the value of n for all temperature range.

$$N = d \ln \sigma_t / d \ln \epsilon \quad \text{Eqn. 7}$$

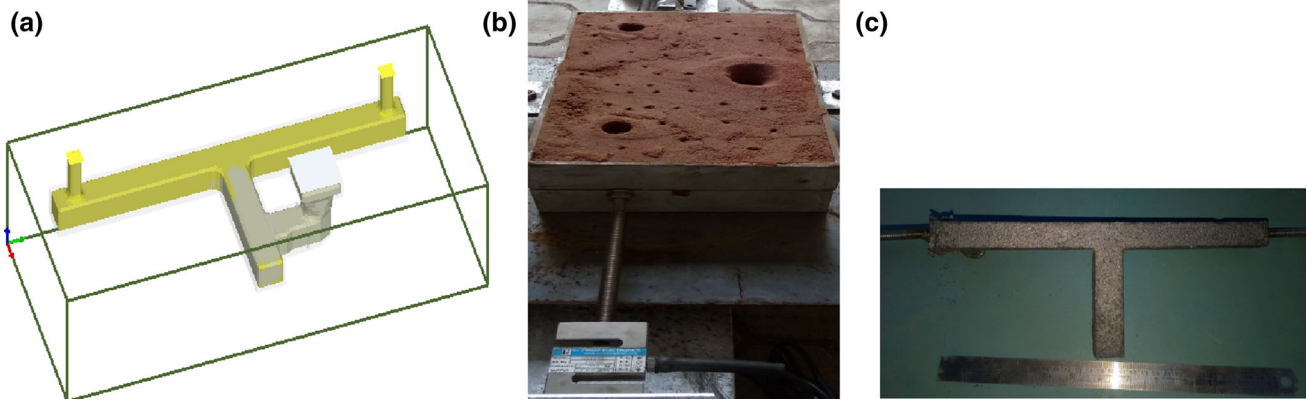


Figure 12. (a) Casting simulation 3D model along with gating system, (b) sand mold with cope and drag with gating system for T-shaped cavity, and (c) actual experimental T-shaped casting.

Table 3. Material Properties of CO₂ sand Mold and Cast Steel CF3M

Sr. no.	Properties	Mold	Cast steel (SS316L)
1	Density (kg/m ³)	1770	8000
2	Liquid density (kg/m ³)	–	7800
3	Thermal conductivity (W/m–K)	0.98	16
4	Specific heat (J/kg-K)	735	514
5	Compressive strength (kPa)	20	–
6	Thermal expansion (µm/m–K)	2.50	15.90
7	Permeability (cm ² /mbar-min)	150	–
8	Tensile strength (MPa)	–	605
9	Fluidity (mm)	–	600

where σ_t = true stress and ε = true strain

$$n = 0.2436 - 5.98 \times 10^{-5} T$$

$$f_{\%c} = 4.655 \times 10^4 + 7.14 \times 10(\%c) + 1.2 \times 10^4(\%c)^2$$

$$\sigma_o = (130.5 - 5.128 \times 10^{-3} T) \cdot \dot{\varepsilon}_{eq}^{f_2}$$

$$f_2 = -0.6289 + 1.114 \times 10^{-3} T$$

$$T(^{\circ}C), \sigma_{eq}, \sigma_o(Mpa)$$

The input parameters are stress, strain, temperature and percentage of carbon, and the output is the viscoplastic strain. The analysis results show that the viscoplastic strain

is an important factor for the occurrence of hot tearing. Therefore, the hot tear can be determined from the stress–strain curve. The constitutive equations help to model the material above the solidus temperature where steel alloy, i.e., CF3M, enters into dynamic strain aging regime. A stress–strain relationship in order to determine flow stresses and hot tear susceptibility has been successfully deduced. Derived constitutive equation will be used in finite element analysis for the alloy modeling at elevated temperature and also validation with experimental results.

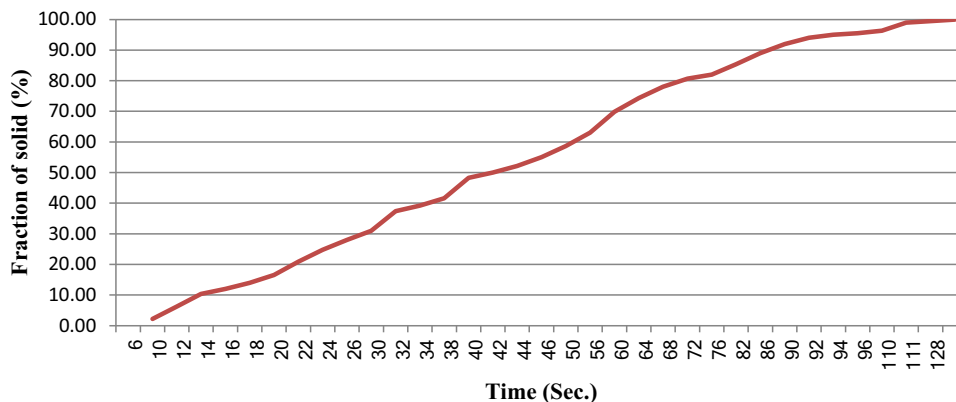


Figure 13. Fraction of solid with respect to time.

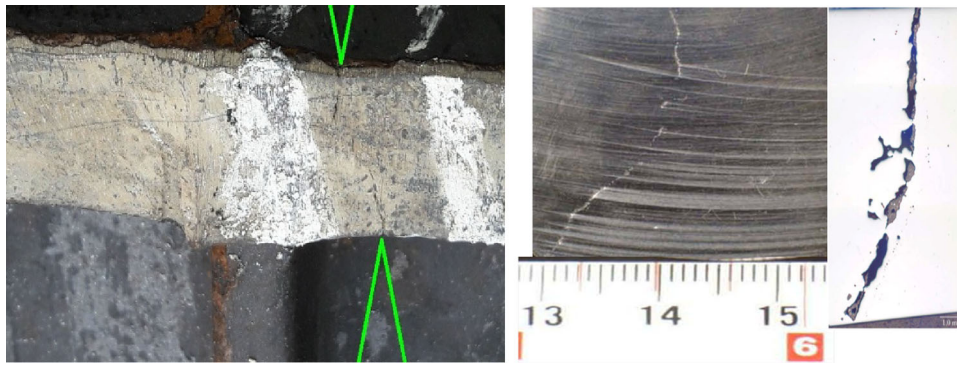


Figure 14. Crack morphology, surface: wide and discontinuous (jagged), Face: very dark (oxidized) and featuring dendritic regions, cross section: darkly oxidized, deep, wide, discontinuous, lined with silicates.

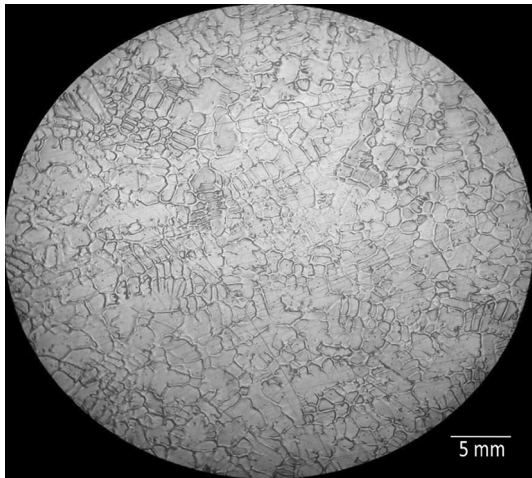


Figure 15. Dendritic structure in 100 × magnification of cut sample.

Casting Simulation

Temperature-dependent heat transfer and mechanical material properties of CF3M are shown graphically in Figure 11; data were calculated using J-Mat Pro-V software for stainless steel as per chemical composition of the

tested sample. It is observed that as temperature increases, the thermal conductivity, expansion coefficient, Poisson's ratio and specific heat increase. Similarly, density and Young's modulus decrease. As the force and displacement were density and Young's modulus driven parameters. To know thermo-physical properties between solidus and liquidus temperatures is important in order to predict the casting behavior in the hot zone. Casting simulation 3D model along with gating system, sand mold with cope and drag having gating system for T-shaped cavity and actual casting are depicted in Figure 12a–c, respectively.

The T-shaped model and its sodium-silicate-bonded silica sand mold were simulated using casting simulation software Auto-CAST-XI, properties assigned to cast steel CF3M was obtained from thermo-physical properties calculations and SiO₂ sand mold cured by CO₂ properties are derived from previous experimental results and software database are shown in Table 3. Pouring temperature is 1560 °C, and an interfacial heat transfer coefficient (IHTC) value between metal and mold, metal(liquid) and air and metal (solid) and air is 925.5 W/m²-K, and that between mold and air was 500 W/m²-K. Total filling time is 1.80 s. The average pouring rate is 1.2 kg/s. Results of the casting

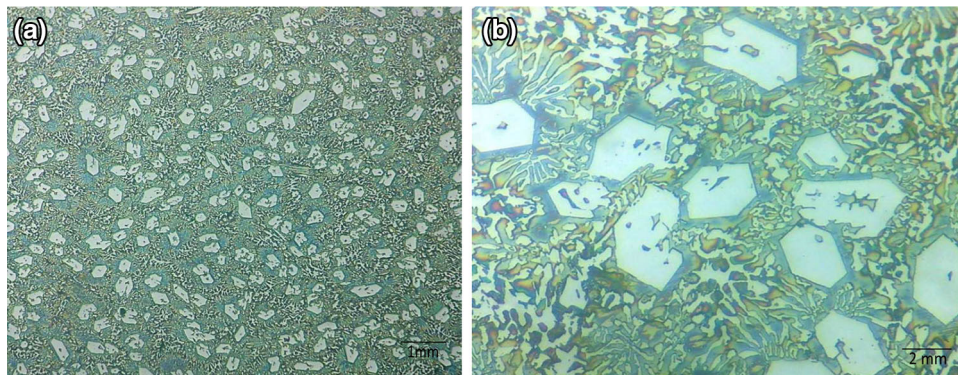


Figure 16. Microstructure in (a) 100 × magnification of sample (b) 500 × magnification of sample.

simulations from pouring temperature to the solidus temperature are shown in Figure 13 graphically. Graphs show solid fraction with respect to time. Simulation results are as follows: solidification time is 3 min and hot cracking susceptibility (HCS) as per Clyne and Davies criteria⁸ derived from calculation is 0.98.

Microscopy

The results of samples found after the cut, mounted, polished and etched are shown in Figure 14. The crack morphology revealed that the surface was wide and discontinuous (jagged), face observed was very dark (oxidized) and has featuring dendritic regions, and the cross section was darkly oxidized, deep, wide, discontinuous, lined with silicates. Figure 15 shows the cut section showing dendritic structure after full solidification and reveals how the bridging of dendrite forms. Also it shows the journey from coherence and coalescence to rigidity temperature. Figure 16 shows the microstructure analysis in 100 × and 500 × magnifications, and microstructure shows ferrite in a matrix of austenite with few precipitated particles of carbides. Defect like the hot tear was easily recognized from characteristics; its form is that of a ragged, branching crack, generally following intergranular paths. This is particularly clear on a polished section viewed under the microscope, the failure surface reveals a dendritic morphology, and the failure surface is often heavily oxidized. Its location is often at a hot spot where contraction strain from adjoining extensive thinner sections may be concentrated; it does not always appear under apparently identical conditions; in fact, it seems subject to a considerable degree of randomness in relation to its appearance or non-appearance, and to its extent. In steels, if the crack is open to the atmosphere, the color of its surface was a useful guide to when it formed: an uncolored metallic surface will indicate that the crack occurred at a temperature near to room temperature; the normal 'temper colors' (the light interference colors reflecting the thickness of the oxide) range from light straw, formed at somewhere near 300 °C, through yellow, blue and finally to brown indicate greater exposure to time at temperature, with temperatures probably approaching 600 or 700 °C for the darker colors.

Conclusion

In the present study, developed apparatus used for in situ casting experiments was equipped with T-shaped mold and instruments with real-time data recording were used to characterize, develop and quantify the hot tearing of alloy similar to type CF3M during solidification. Using this method, it becomes possible to determine the stress, strain and temperature along with solid fraction at which hot tearing occurs. The onset of hot tearing can be determined

from stress versus strain curve. The amount of shrinkage/contraction can be quantitatively measured.

The temperature difference and the time duration in the stress release process are 7 °C and 4 s, respectively, solid fraction is about 16%, which confirms the process of the tear formation and healing. Repeated stress release is observed in the same sample in the temperature range of 1431–1421 °C; at that time the solid fraction is around 50% and time duration of 4 s is observed. When the solid fraction in the core approaches 50%, molten steel in the core is at mushy state. At this time, the hot tearing susceptibility of the sample is largest. The sample was torn at second stress release point, and the first fluctuation represents the healed hot tear. This study suggested that the strain or strain rate is more critical for hot tearing than stress. The studies on residual stress show that the tensile stress is not required to generate hot tears, but only tensile strain is sufficient to form a hot tear. The strain-based criteria compare the proposed critical strain and the experimentally measured ductility of the alloy. If a calculated critical strain is higher than the experimentally determined fracture strain, hot tearing will occur. Residual stress analysis performed using sectioning method by cutting specimen revealed that the torn casting has negligible residual stress in it. Our investigations into this area of residual stress of torn casting are still ongoing using FTIR and strain gauges and mathematical modeling for same.

Microscopic study revealed the crack morphology; hot tear had a jagged pattern, darkly oxidized, and lined with silicates. For the open crack, the color of its surface was a useful guide to know when it formed.

Compliance with Ethical Standards

Conflict of interest The authors declare that they have no conflict of interest.

REFERENCES

1. J. Campbell, *Castings* (Butterworth and Heineman Ltd, Oxford, 1991)
2. C.L. Martin, D. Favier, M. Suery, *Int. J. Plast.* **15**, 981–1008 (1999)
3. Y. Wang, B. Sun, Q. Wang, Y. Zhu, W. Ding, *Mater. Lett.* **53**, 35–39 (2002)
4. O. Ludwig, J.M. Drezet, C.L. Martin, M. Suery, *Metall. Mater. Trans. A* **36**, 1525–1535 (2005)
5. M. Rappaz, J.-M. Drezet, M. Gremaud, *Metall. Mater. Trans.* **30A**, 449–455 (1999)
6. H.F. Bishop, C.G. Ackerlind, W.S. Pellini, *Metallurgy and mechanics of hot tearing*. AFS Trans. **60**, 818–833 (1952)
7. B.G. Thomas, *Modeling of Stress, Distortion and Hot Tearing* ASM Handbook, Volume 15: Casting ASM

- Handbook Committee, pp. 449–461.
<https://doi.org/10.1361/asmhba0005238>
8. T.W. Clyne, G.J. Davies, A quantitative solidification test for castings and an evaluation of cracking in aluminium–magnesium alloys. *Br. Foundryman* **68**, 238 (1975)
 9. S. Li, D. Apelian, Hot tearing of aluminum alloys. *Int. Metalcast.* **5**(1), 23–40 (2011).
<https://doi.org/10.1007/BF03355505>
 10. N. Hatami, R. Babaei, M. Dadashzadeh, P. Davami, J. Mater. Process. Technol. **205**, 506–513 (2008)
 11. J.Z. Zhu, J. Guo, M.T. Samonds, *Int. J. Numer. Methods Eng.* **87**, 289–308 (2011)
 12. Z. Wang, J. Song, Y. Huang, A. Srinivasan, Z. Liu, K. Kainer et al., *Metall. Mater. Trans. A* **46**, 2108–2118 (2015)
 13. M. Alvarez Vera, J.H. Garcia-Duarte, A. Juarrez-Hernandez, R.D. Mercado-Solis, A.G. Castillo, M.A.L. Hernandez-Rodriguez, Failure analysis of Co–Cr hip resurfacing prosthesis during solidification. *Case Stud. Eng. Fail. Anal.* **1**, 1–5 (2013)
 14. M. Pokorny, C. Monroe, C. Beckermann et al., *Int. Metalcast.* **2**, 41 (2008).
<https://doi.org/10.1007/BF03355435>
 15. C.A. Monroe, C. Beckermann, J. Klinkhammer, *Modeling of Casting, Welding, and Advanced Solidification Process-XII* (TMS, Warrendale, 2009), pp. 313–320
 16. S. Kou, *JOM* **55**, 37 (2003).
<https://doi.org/10.1007/s11837-003-0137-4>
 17. S. Kou, *Acta Mater.* **88**, 366–374 (2015)
 18. Z. Lin, A. Monroe, C.K. Huff, R.C. Beckermann, Prediction of hot tear defects in steel castings using a damage based model. *Model. Cast. Weld. Adv. Solid. Process.* **12**, 329–336 (2009)
 19. J.C. Hamaker, W.P. Wood, Influence of phosphorus on hot tear resistance of plain and alloy gray iron. *AFS Trans.* **60**, 501–510 (1952)
 20. J.V. Eeghem, A.D. Sy, A contribution to understanding the mechanism of hot tearing of cast steel. *AFS Trans.* **73**, 282–291 (1965)
 21. S.A. Metz, M.C. Flemings, A fundamental study of hot tearing. *AFS Trans.* **78**, 453–460 (1970)
 22. Y.F. Guven, J.D. Hunt, Hot-tearing in aluminum copper alloys. *Cast. Met.* **1**, 104–111 (1988)
 23. Z.-Q. Wei, X.-R. Chen, H.-G. Zhong, Q.-J. Zhai, G. Wang, Hot tearing susceptibility of Fe–20.96Cr–2.13Ni–0.15N–4.76Mn–0.01Mo duplex stainless steel. *J. Iron Steel Res. Int.* **24**, 421–425 (2017)
 24. Z. Li, H. Zhong, Q. Sun, X. Zhengqi, Q. Zhai, Effect of cooling rate on hot-crack susceptibility of duplex stainless steel. *Mater. Sci. Eng. A* **506**, 191–195 (2009)
 25. A. Stangeland, A. Mo, M. M’hamdi, D. Viano, C. Davidson, Thermal strain in the mushy zone related to hot tearing. *Metall. Mater. Trans.* **37**, 705 (2006)
 26. H. Akhyar, V. Malau, P.T. Iswanto Suyitno, Hot tearing susceptibility of aluminum alloys using CRCM-horizontal mold. *Results Phys.* **7**, 1030–1039 (2017)
 27. D.S. Bhiogade, S.M. Randiwe, A.M. Kuthe et al., Study of hot tearing in stainless steel CF3M during casting using simulation and experimental method. *Int. Metalcast.* **12**, 331–342 (2018).
<https://doi.org/10.1007/s40962-017-0170-7>
 28. A.S. Sabau, S. Mirmiran, S. Li et al., *Hot-tearing assessment of multicomponent nongrain-refined Al–Cu alloys for permanent mold castings based on load measurements in a constrained mold* (Met. Mater. Soc. ASM Int., Miner, 2018).
<https://doi.org/10.1007/s11663-018-1204-0>
 29. R. Tuttle, Examination of steel castings for potential nucleation phases. *Int. Metalcast.* **4**(3), 17–25 (2010).
<https://doi.org/10.1007/BF03355495>
 30. A. Roger, Stainless steel: an introduction to their metallurgy and corrosion resistance. *Dairy Food Environ. Sanit.* **20**(7), 506–517 (2000)
 31. J. Thorborg, J. Klinkhammer, M. Heitzer, Transient and residual stresses in large castings, taking time effects into account. *IOP Conf. Ser. Mater. Sci. Eng.* **33** (2012). <https://doi.org/10.1088/1757-899X/33/1/012050>
 32. N.S. Rossini, M. Dassisti, K.Y. Benyounis, A.G. Olabi, Methods of measuring residual stresses in components. *Mater. Des.* **35**, 572–588 (2012)
 33. G. Palumbo, V. Piglionico, Modelling residual stresses in sand-cast superduplex stainless steel. *J. Mater. Process. Technol.* (2014).
<https://doi.org/10.1016/j.jmatprotec.2014.11.006>
 34. M.B. Prime, Cross-Sectional Mapping of residual stresses by measuring the surface contour after a cut. *J. Eng. Mater. Technol.* **123**(2), 162–168 (2001)